Global Biogeochemical Cycles®

Key Points:

- Globally, C turnover time ranges between 1 and 1,000 years in wetlands
- The Carbon cycle is driven by anaerobic respiration in 78% of the global wetlands, by aerobic in 15%, and by destabilization from soil minerals in 5%
- The turnover time changes up to two orders of magnitudes within the season in the northern regions, rising concern for future high emissions

Supporting Information:

Supporting Information may be found in the online version of this article.

Correspondence to:

C. Pasut and F. Maggi,
chiara.pasut@csiro.au;
federico.maggi@sydney.edu.au

Seasonal Biotic Processes Vary the Carbon Turnover by Up To One Order of Magnitude in Wetlands

Chiara Pasut[1,2], Fiona H. M. Tang[3,4] [ID], Budiman Minasny[5] [ID], Charles R. Warren[5] [ID], Feike A. Dijkstra[5] [ID], William J. Riley[6] [ID], and Federico Maggi[1]

[1]Environmental Engineering, School of Civil Engineering, The University of Sydney, Sydney, NSW, Australia, [2]CSIRO Agriculture & Food, Urrbrae, SA, Australia, [3]Department of Crop Production Ecology, Swedish University of Agricultural Sciences (SLU), Uppsala, Sweden, [4]School of Environmental and Rural Science, University of New England, Armidale, NSW, Australia, [5]School of Life and Environmental Sciences, Sydney Institute of Agriculture, The University of Sydney, Sydney, NSW, Australia, [6]Earth Sciences Division, Lawrence Berkeley National Laboratory, Berkeley, CA, USA

Abstract Soil Organic Carbon (SOC) turnover τ in wetlands and the corresponding governing processes are still poorly represented in numerical models. τ is a proxy to the carbon storage potential in each SOC pool and C fluxes within the whole ecosystem; however, it has not been comprehensively quantified in wetlands globally. Here, we quantify the turnover time τ of various SOC pools and the governing biotic and abiotic processes in global wetlands using a comprehensively tested process-based biogeochemical model. Globally, we found that τ ranges between 1 and 1,000 years and is controlled by anaerobic (in 78% of global wetlands area) and aerobic (15%) respiration, and by abiotic destabilization from soil minerals (5%). τ in the remaining 2% of wetlands is controlled by denitrification, sulfur reduction, and leaching below the subsoil. τ can vary by up to one order of magnitude in temperate, continental, and polar regions due to seasonal temperature and can shift from being aerobically controlled to anaerobically controlled. Our findings of seasonal variability in SOC turnover suggest that wetlands are susceptible to climate-induced shifts in seasonality, thus requiring better accounting of seasonal fluctuations at geographic scales to estimate C exchanges between land and atmosphere.

Plain Language Summary Wetlands are the greatest sink of carbon globally. The time spent by soil organic carbon within wetlands (called turnover time) in response to hydroclimatic forces is the focus of extensive debate. This is the first global-scale assessment that identifies the key drivers of seasonal changes in soil organic carbon turnover in wetlands. Our findings suggest a higher vulnerability of carbon stock than expected due to seasonal temperature and precipitation changes. Finally, our approach sets the basis to further quantify the response against scenarios of climatic changes.

1. Introduction

The first meter of soil contains the largest global soil organic carbon (SOC) stock (about 1,500 Gt-C, Guo & Gifford, 2002; Jobbágy & Jackson, 2000; Scharlemann et al., 2014). This relatively shallow layer has such a pivotal role in controlling the global atmospheric CO_2 concentration that a loss of 10% of SOC to the atmosphere would be equivalent to 30 years of anthropogenic CO_2 emissions (Kirschbaum, 2000). A large proportion of those SOC losses could stem from wetlands because they cover about 4 to 11.4 million km^2 (Mkm²) globally (including peatlands, forested wetlands, and permanent and seasonal wetlands, Poulter et al., 2017; Schroeder et al., 2015; Z. Zhang et al., 2021) and store almost 20% of global soil C (Lal, 2004; Temmink et al., 2022). The stability of SOC is well represented by the turnover time τ because it gives a measure of the time scale spent by SOC within an ecosystem as a result of trade-offs between C inputs and outputs, and therefore represents the level of activity of SOC (Six & Jastrow, 2002).

Wetlands store proportionally large amounts of SOC because permanent or seasonal anoxic conditions keep C loss through decomposition at low rates and lengthen the C turnover time τ as compared to other ecosystems. However, fast-changing climatic patterns are gradually shifting wetland functioning from a net C sink of atmospheric CO_2 to a net C source, raising concern around the destabilization of SOC stock and its repercussions on atmospheric CO_2 and CH_4 concentrations, particularly on the latter, which has a much stronger greenhouse gas effect than CO_2 (almost 30 times greater over a 100-year timespan).

Visualization: Chiara Pasut
Writing – original draft: Chiara Pasut
Writing – review & editing: Budiman Minasny, Charles R. Warren, Feike A. Dijkstra, William J. Riley, Federico Maggi

While C inputs to soil are generally associated with net primary productivity and deposition from surface processes, losses can occur via multiple biotic (e.g., aerobic and anaerobic respiration, immobilization) and abiotic (e.g., erosion, fires, leaching to deep soil strata, mineral interaction) processes. The simplest and most effective approach to estimate τ is to assume the system is in steady-state, that is, constant SOC stock regardless of whether it is differentiated by pools and assuming that inputs are equal to losses. With these assumptions, τ of various SOC pools in lumped ecosystems (i.e., spatially average representation of the ecosystems present in a unit area) have been estimated to range between 10^{-2} and 10^3 years (Carvalhais et al., 2014; Z. Luo et al., 2019). In particular, low molecular weight dissolved organic carbon (DOC) and free particulate organic carbon (FPOC) have τ values ranging between 10^{-2} and 10^{-1} years (Cotrufo et al., 2019; Dutta & Dutta, 2016; Lavallee et al., 2020) and between 10^0 and 10^1 years (Golchin et al., 1994; Lavallee et al., 2020) respectively. In contrast, τ of mineral-associated and protected organic carbon (MAPOC) can range between 10^0 and 10^3 years (Golchin et al., 1994). However, wetlands are relatively complex compared to upland ecosystems because of seasonal changes in inundation and, consequently, in redox conditions, microbial activity, and plant processes, thus causing variability in heterotrophic and methanogenic respiration rates (Calabrese et al., 2021; Hondula et al., 2021; Macdonald et al., 1998). These issues suggest that τ of SOC in wetlands may vary substantially across seasons.

Here, we hypothesize that τ of SOC in wetlands can dynamically vary across the seasons at a greater amplitude than in other ecosystems that are less affected by seasonality in surface hydrology. We further explore the biotic and abiotic processes dynamically affecting the losses from C pools in wetlands to identify the processes controlling the seasonality of τ across climatic regions.

To test our working hypothesis, we estimate τ of various organic C pools (particulate, dissolved, and mineral associated) in wetlands using a spatially and temporally explicit dynamic model, BRTSim-BAMS4 (Biotic and Abiotic Model for SOM version 4, Pasut et al., 2021), that has been tested against wetland CH_4, CO_2, and N_2O flux tower emissions, and benchmarked to bottom-up and top-down global and regional emission modeling studies (Chang et al., 2021) and C sequestration rates (Pasut et al., 2021). We compute τ with a new approach (Section 2) that extends the framework in Six and Jastrow (2002). Specifically, we analyzed τ by assuming a near-steady state at a monthly time scale, and we explicitly accounted for dynamic biotic and abiotic processes removing C from those pools (see Section 2). The BRTSim-BAMS4 model describes the hydraulics of wetlands and the biogeochemistry of various organic C pools representing several conceptual pools with different molecular structures, varying in C, nitrogen (N) and sulfur (S) content and reactivity to soil minerals (Riley et al., 2014), including monomers (e.g., monosaccharides, fatty acids, amino acids, amino sugars, organic acids, phenols, and nucleotides) and polymers (lignin, cellulose, hemicellulose, and peptidoglycan). We mapped in space and time the rate of biotic processes involved in the coupled biogeochemical C, N, and S cycles and the rate of abiotic processes of advection, diffusion, and mineral protection that contribute to relocating C from and to different pools, and along the soil column. This approach allowed us to track which biotic (CO_2 and CH_4 production) and abiotic processes govern SOC turnover in wetlands and its seasonality. The model was applied to a global grid at 0.5° resolution over a multi-year wetland surface area ranging between 1.2 and 11.4 Mkm^2 for the period between 2000 and 2017, and results were presented along with their certainty.

2. Materials and Methods

2.1. Computational Domain

The computational domain covers an average wetland surface area of 3.8 Mkm^2 (ranging between 1.2 and 11.4 Mkm^2 from 2000 to 2017) described by about 45,000 grid cells at a grid resolution of 0.5° (about 50 km at the equator). Grid cells covered by wetlands for at least 2% of the total grid cell area were selected from the SWAMPS v3.2 wetlands database (Poulter et al., 2017), which reported the monthly flooded land area from 2000 to 2017 based on active and passive microwave satellite images excluding lakes, reservoirs, rivers, and saline environments. Each selected grid cell is represented by a 2 m atmospheric column that includes four atmospheric layers necessary for heat and gas exchanges, and water flooding (30, 30, 40, and 100 cm thick from land surface upward), one layer of the top soil (0–30 cm), two layers of subsoil (30–100 cm), and one layer below the first meter of soil (100 cm thick). Each grid cell is characterized by a depth-specific soil bulk density, porosity, and textural soil fractions (Poggio et al., 2021), hydraulic and thermal conductivity, heat capacity, air-entry potential, and pore volume distribution index (Dai et al., 2013). This study does not include wetland connectivity and

lateral flows. All data used to parameterize the computational domain are listed in Table S2 of the Supporting Information in Pasut et al. (2021).

2.2. Hydrological Model

Water dynamics within the computational domain explicitly accounted for precipitation (P), evapotranspiration (ET), and land runoff (RNF) calculated using the Curve Number model (Rallison, 1980) and implemented as in Pasut et al. (2021). P, ET, and RNF were used to quantify the annual water budget in each grid cell (WB = $P - ET + \Delta RNF$) and introduce an additional flux (FB = $-WB$) associated with the water budget to prevent the sequence of finite volumes defining each grid cell of the computational domain to become fully dry or fully saturated when WB $\neq$ 0. FB was introduced as a constant flux throughout the year, but was variable across the years during a simulation, and therefore FB did not affect the intra-day or seasonal water table fluctuations. Within the finite volumes of the computational domain, the hydrological model accounted for heat and water flow in variably saturated conditions using the Richards' equation with the Brooks and Corey model of the soil saturation, water potential, and hydraulic conductivity relationships (Brooks & Corey, 1964).

2.3. Biogeochemical BAMS4 Model

We described SOC with five organic C pools: PolyC represents lignin, cellulose, and hemicellulose organic polymers; PolyCN represents peptidoglycan; MonoC, MonoCN, and MonoCS are three low molecular weight organic monomers containing C, C and N, and C and S, respectively, representing monosaccharides, fatty acids, organic acids, phenols, amino acid, amino sugar, and nucleotides resulting from root exudates, and depolymerization of PolyC and PolyCN, which contain C, and C and N, respectively (Table S1 in Supporting Information S1). We also included two C pools representing CH_4 and CO_2. Four microbial functional groups control the C cycle: fungi F_{DEP} are responsible for the depolymerization of PolyC; heterotrophs B_{AER} are responsible for aerobic respiration on MonoC, MonoCN, MonoCS, and PolyCN; methanogens B_{MGB} are responsible for anaerobic respiration on MonoC; and methanotrophs B_{MOB} are responsible for CH_4 oxidation. The C cycle was coupled with the N and S cycles to account for the feedback introduced by e- donors and acceptors on the biotic response of each elemental cycle (Figure S6 in Supporting Information S1). Specific to the N cycle, we accounted for atmospheric N_2 fixation, NH_4^+ nitrification by ammonia oxidizers B_{AOB} and nitrite oxidizers B_{NOB}, and NO_2^- and NO_3^- denitrification mediated by denitrifiers B_{DEN}. For S, we accounted for reduction, disproportion, and oxidation reactions mediated by sulfur S reducers B_{SrRB}, thiosulfate and sulfite ($S_2O_3^{2-}$, SO_3^{2-}) reducers B_{ThSRB}, sulfate SO_4^{2-} reducers B_{SRB}, $S_2O_3^{2-}$, and SO_3^{2-} disproportioning microbes B_{SDB}, and photolithoautotroph oxidizers B_{SOB}. Each of the organic and inorganic C, N, and S pools can be in the aqueous and gaseous phases, or minerally associated, that is, protected from biological activity. All the biochemical reactions and corresponding parameters are presented in Supplementary Information in Pasut et al. (2021).

Diffusion and advection of aqueous and gaseous species are modeled using the Fick's and Darcy's laws, respectively. Gas dissolution and volatilization are modeled using the mass action law at local equilibrium (Maggi, 2021). Mineral association and destabilization of MonoC, MonoCN, MonoCS to the soil matrix is described by two-way first-order kinetics with forward to backward ratio as in Riley et al. (2014). The biologically mediated reactions are described by the generalized Michaelis-Menten-Monod kinetics (Michealis & Menten, 1913; Monod, 1966) at each soil depth. The microbial response is moderated by soil pH, O_2 availability, water saturation S, and temperature T. The pH constraint is accounted for by a Michaelis-Menten term for pH = 8 and by an inhibition term for pH = 5 (Boon & Laudelout, 1962; Paul, 2014), while dissolved O_2 inhibits (in order of strength) denitrification, sulfur reduction, and methanogenesis. The biological response to S and T is accounted for as $f_B = \min\{f_T, f_S/\max\{f_S\}\}$, where

$$f_T = \left(\frac{e^T}{e^{T_L} + e^T} \right)^{0.15} \times \left(\frac{e^{T_U}}{e^{T_U} + e^T} \right)^{0.35}, \qquad (1)$$

$$f_S = \left(\frac{S}{S_L + S} \right) \times \left(\frac{S_U}{S_U + S} \right). \qquad (2)$$

Here, T_L = 13°C and T_U = 37°C are the lower and upper response temperatures for mesophiles (Rittmann & McCarty, 2001; Wickland & Neff, 2008), while $S_L = S_U$ = 0.46 are the lower and upper response saturations

estimated after (Wickland & Neff, 2008). The fungi have a C:N ratio of 8:1 and other microbial functional groups have a C:N ratio of 5:1 (Rittmann & McCarty, 2001). Necromass decomposition returns the assimilated C and N to the soil as MonoC, MonoCN, and PolyCN. Plant uptake of NH_4^+, NO_3^-, SO_4^{2-}, and PO_4^{3-} is modeled by Michaelis-Menten kinetics, while CH_4 transport from the soil to the atmosphere by some vascular plants was described by diffusion through aerenchyma (after Walter et al., 2001). Each grid cell is characterized by vegetation-dependent average plant root density profile with average depth calculated based on Canadell et al., (1996) and Paul (2014).

2.4. Initial and Boundary Conditions

The water saturation was initialized using the Soil Moisture data set by NOAA/OAR/ESRL PSD, Boulder, Colorado, USA (Rodell et al., 2004), and the near-surface atmospheric temperature was initialized with the long-term January average of the CRU-TS3.21 data set (Harris et al., 2020). The soil C in BAMS4 was initialized as mineral-associated MonoC, MonoCN, and MonoCS at C:N ratio of 13 and C:S ratio of 74, and with the total C as in SoilGrids v2 (Poggio et al., 2021).

The boundary conditions include daily precipitation, monthly S and N atmospheric deposition (Seiji et al., 2019), daily long- and short-wave up- and downwelling solar radiation (Climatic Research Unit—CRU-TS 3.21- Harris et al., 2020), monthly evapotranspiration (Y. Zhang et al., 2016), and weekly net primary productivity (NPP) (Moderate Resolution Imaging Spectroradiometer, MODIS Land Science Team, 2019) from 2000 to 2017. The organic C inputs to soil were based on the NPP and reduced by 30% assuming losses due to fire and other anthropogenic sources (Harden et al., 2000). The quality of organic matter inputs to soil was assigned by C:N:S ratio of the above- and below-ground litter, and the below-ground litter entered the soil following the root density profile. Specifically, the corresponding values of each above variables were derived by merging the land cover map (MODIS- LC, Sulla-Menashe et al., 2019) and literature values (Bréchet et al., 2017; Hättenschwiler & Jørgensen, 2010; Pei et al., 2019; Rouifed et al., 2010; Snowdon & Ryan, 2005). N_2 fixation was not described as a biological reaction, but its rate was explicitly made dependent on temperature, pH, and water availability with rate constant from Paul (2014). More details can be found in Pasut et al. (2021). All boundary flows and data were harmonized at $0.5° \times 0.5°$ resolution with either a mass-conservative interpolation for quantities related to mass or energy (e.g., precipitation, solar radiation, and NPP) or a linear interpolation otherwise (e.g., hydraulic conductivity and porosity). The data sets for the boundary conditions are listed in Supporting Information S1 (Table S2).

2.5. Computational Environment and Spin-Up

The hydrological and biogeochemical models were numerically solved within the general-purpose multi-phase and multi-species bioreactive transport simulator BRTSim-v5.0b, which couples in a hybrid explicit-implicit way the mass and energy conservation and continuity laws of the liquid and gas phases, energy (heat), dissolved and minerally associated species, and biological species within finite volumes and with a variable integration time step. Details are reported in the User Manual and Technical Guide (Maggi, 2021).

We ran a spin-up of 500 years by re-looping the time sequences of boundary conditions from 2000 to 2017 to reach a dynamic steady state of the biogeochemical fluxes and sizes of the soil C pools. Steady-state was detected if the difference in C pool size was less than or equal to 1 gC m^{-2} in two consecutive 18-year time windows. We used the last 18 years for the analyses in this study.

2.6. C Pool Aggregation for Analyses

The organic C pools in BAMS4 were aggregated into four classes for the purpose of analyses and communication of results: dissolved organic carbon (DOC) includes aqueous MonoC, MonoCN, and MonoCS; free particulate organic carbon (FPOC) includes PolyC and PolyCN in solid phase; mineral-associated and protected organic carbon (MAPOC) includes MonoC, MonoCN, MonoCS in mineral phase; and, total soil organic C (SOC), which includes all above (Table S1 in Supporting Information S1). FPOC and MAPOC are not subject to diffusion and advection (Figure S6 in Supporting Information S1).

We analyzed the geographic distribution of aggregated pools in arid, tropical, temperate, continental, and polar regions using the first level classification of Köppen and Geiger (Kottek et al., 2006) (Figure S7 in Supporting Information S1). We calculated the monthly C mass fraction (gC kgsoil^{-1}) and turnover τ (year) of each SOC pool

in topsoil and subsoil, and climatic regions, and their long-term monthly and annual average, median, standard deviation, and 25th and 75th percentiles.

2.7. Estimation of the Turnover Time τ

We tracked the size $C_i(y, m, z)$ of DOC, FPOC, and MAPOC pools and the fluxes $F_{i,j}(y, m, z)$ that remove C from each pool i in a given year y, month m, and depth z to calculate their turnover time τ_i. The jth flux includes aerobic respiration (F_{Aer}) and anaerobic respiration (F_{Ana}), DOC oxidation during denitrification (F_{Den}) and sulfur reduction (F_{Sulf}), the leaching of DOC below z (F_{Leach}), and mineral association of DOC (F_{Ma}) or destabilization of MAPOC (F_{Dest}) (Table S1 in Supporting Information S1). The biogeochemical system at dynamic steady state implies that the pool size $C_i(y, m, z)$ in a given year y, month m, and depth z varies seasonally at the monthly time scale, that is, $C_i(y, m, z) \neq C_i(y, n \neq m, z)$ for months $n \neq m$, but variations in the same month m of two different years $w \neq y$ are substantially smaller, that is, $C_i(y, m, z) \approx C_i(w \neq y, m, z)$. This may not necessarily apply to individual fluxes $F_{i,j}$ because these are susceptible to seasonal conditions (e.g., redox in biotic processes) but it may apply to the sum of all the fluxes. Upon the assumption that these annual variations in C_i in corresponding months are negligible, that is, $C_i(y, m, z) = C_i(w \neq y, m, z)$, we can expand the theory in Six and Jastrow (2002) and define the turnover time τ_i in pool i, month m, and depth z as

$$\tau_i(m, z) = \frac{C_i(m, z)}{\sum\limits_j F_{i,j}(m, z)},$$
(3)

where $\sum_j F_{i,j}$ is the sum of all the fluxes j from a pool C_i. The depths z of interest in this work are the topsoil (0–30 cm) and subsoil (30–100 cm).

We calculated the long-term monthly average of each flux from 2000 to 2017 for each climatic region to detect possible patterns and shifts between major fluxes. The fluxes were then weight averaged for the actual wetland extension during a specific month.

Differences and similarities across variables and between climatic regions and C pool were tested with a one-way ANOVA and a post-hoc test to determine their statistical significance (set at $p < 0.01$). For large sample size such as in this work, one-way ANOVA is assumed to be robust even against the violation of the assumption of normality and homogeneity (Feir-Walsh & Toothaker, 1974). The Pearson coefficient (R) was used to analyze the linear correlation of τ of each C pool with the temperature, precipitation, NPP, and the biotic and abiotic processes involved in the C turnover. For this analysis, we considered the annual average of each variable of interest during the period 2000 and 2017 and statistical significance of $p < 0.01$.

2.8. Certainty Analysis

The assumption of dynamic steady state in C_i and the monthly variability in $F_{i,j}$ introduces uncertainties in our estimates. Hence, we randomly extracted 2,000 independent samples of C_i and $\sum_{i,j} F_{i,j}$ from a Gaussian distribution in each grid cell and for each month, and we re-calculated τ using Equation 3. Next, each month m is assigned with a percentile certainty $\delta_p(m) = 1$ if the calculated (deterministic) τ values sit within the nth percentile window $p^n = (p_L^n, p_U^n)$ of lower and upper percentiles for more than 50% of the time throughout the assessment period from 2000 to 2017, otherwise is assigned with a percentile certainty $\delta_{p^n}(m) = 0$, that is

$$\delta_{p^n}(m) = \begin{cases} 1 & \text{if } \left(p_L^n \leq \tau \leq p_U^n\right) \text{for more than 50\% of the time} \\ 0 & \text{otherwise} \end{cases}.$$
(4)

For this analysis, we used $n = 6$ percentile pairs with bounds (5th, 95th), (10th, 90th), (15th, 85th), (20th, 80th), (25th, 75th), (30th, 70th), (35th, 65th), and (40th, 60th). Next, we calculated the certainty index (Δ) as the average of the outcomes in Equation 4 as

$$\Delta(m) = \frac{\sum\limits_n \delta_{p^n}}{n},$$
(5)
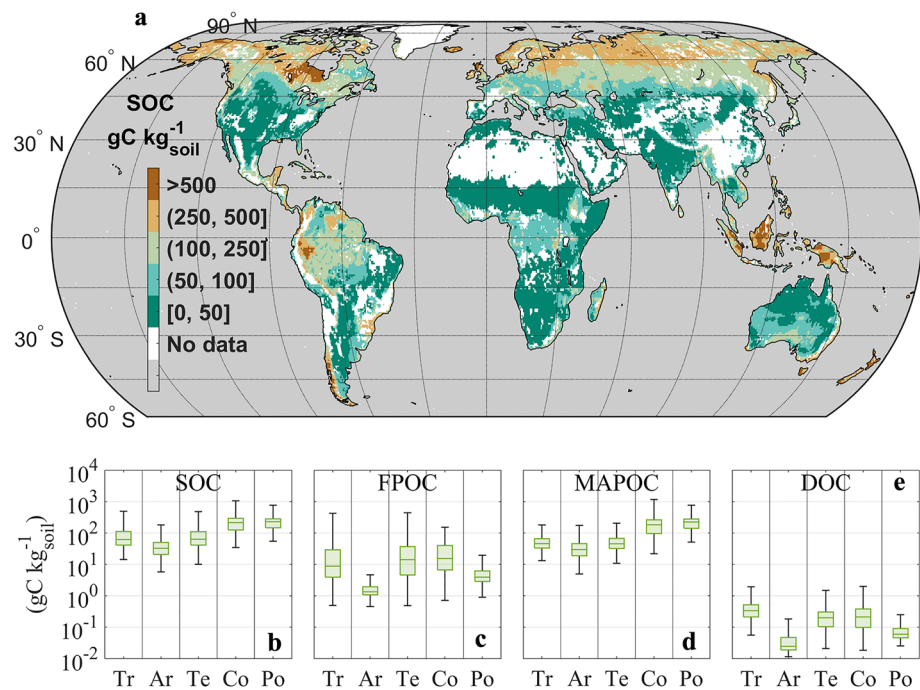
Figure 1. Global spatial distribution of wetland soil organic carbon (SOC) content. (a) Geographic distribution of SOC in the top meter of soil. (b) Soil organic carbon (SOC), (c) free particulate organic carbon (FPOC), (d) mineral-associated and protected organic carbon (MAPOC), and (e) dissolved organic carbon (DOC) in each climatic region. Tr, Ar, Te, Co, and Po indicate tropical, arid, temperate, continental, and polar climatic regions, respectively. The box plot represents the 25th and 75th percentiles, the horizontal solid line represents the median, and the vertical whisker represents the range.

where Δ ranges from 0 (least certain) to 1 (most certain). Significant values of the certainty index are identified when $\Delta \geq 0.75$, and signifies that the estimated turnover time is reliable.

Figure S4 in Supporting Information S1 shows the percent of grid cells in each climatic region that are certain in each month ($\Delta \geq 0.75$) and the spatial and temporal variability of Δ, respectively. The least certain areas, particularly during the cold months, are the Northern latitudes (above 60°N), which became more certain during spring and summer time.

3. Results

3.1. The Spatial Distribution of Soil Organic Carbon

The predicted long-term average SOC content in the top meter (0–100 cm) of global wetlands ranges between 40 and 600 gC kgsoil^{-1} and can vary 15-fold geographically (Figure 1a) and 2.8-fold along the soil profile, with the topsoil (TS, 0–30 cm) storing 71% of the C within the top meter of soil (Figures S1a and S1b in Supporting Information S1). SOC in wetlands consists of a spatial and temporal average of 84% MAPOC, 16% FPOC, and less than 1% DOC. MAPOC globally ranges between 5 and 500 gC kgsoil^{-1}, FPOC between 0.06 and 200 gC kgsoil^{-1}, and DOC between 0.01 and 1 gC kgsoil^{-1} (Figures 1c–1e).

Polar (referred to as high-latitude regions) and continental regions have the greatest C content (greater than 400 gC kgsoil^{-1}), and 80% of it consists of MAPOC. In contrast, the arid region shows the smallest C content, on average 22 gC kgsoil^{-1}, which is mostly in the form of MAPOC. The tropical region has the third greatest C content, on average 150 gC kgsoil^{-1}, almost evenly distributed between MAPOC and FPOC. A one-way ANOVA analysis followed by a post-hoc test showed statistically significant differences ($p < 0.01$) in C content across pools and climatic regions (Figure S2 in Supporting Information S1).

3.2. Long-Term Average τ of SOC, DOC, MAPOC, and FPOC

The long-term average wetland turnover time ranges from less than 1 year in the tropical region to more than 1,000 years in the polar region (Figure 2a), with a global average of 400 years. τ is the largest above 60°N and
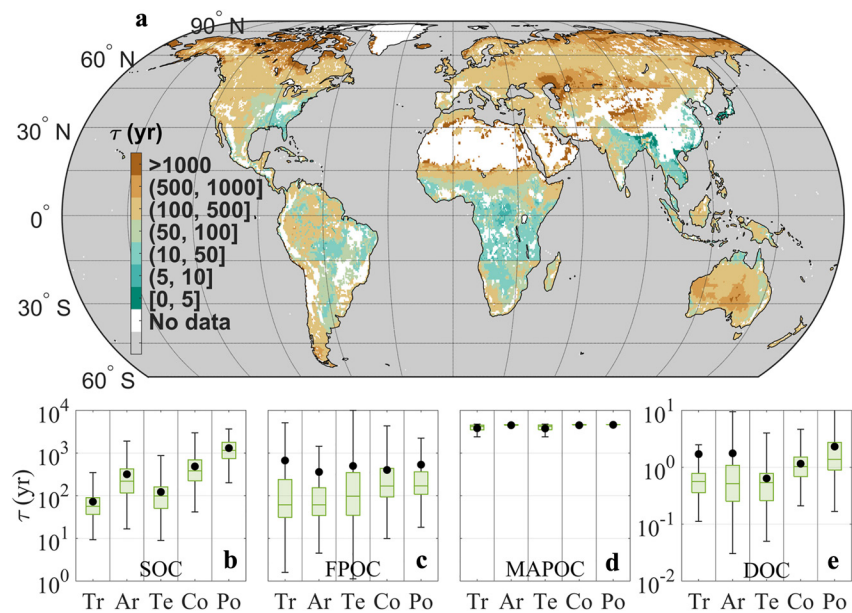
Figure 2. Long-term average turnover times τ. (a) Geographic distribution of τ in the top meter of soil. Panels (b)–(e) represent the turnover time of soil organic carbon (SOC), free particulate organic carbon (FPOC), mineral-associated and protected organic carbon (MAPOC), and dissolved organic carbon (DOC) in each climatic region, with Tr, Ar, Te, Co, and Po representing the tropical, arid, temperate, continental, and polar climatic regions, respectively. The box plot represents the 25th and 75th percentiles, the horizontal solid line represents the median, the black dot represents the average, and the vertical whiskers represent the full range.

below 50°S, and at the edge of the Sub-Saharan, central Asia, and Australian deserts (arid region). In general, we found the SOC in the topsoil turns over 1.2 times faster than in subsoil (Figure S3 in Supporting Information S1).

The turnover of soil C represented in Figure 2 combines τ_{DOC}, which is on average the fastest (2 weeks–10 years), followed by τ_{FPOC} (<1 week to >1,000 years), and lastly, τ_{MAPOC} (3,000–6,000 years) (Figures 2c–2e). The τ_{DOC} and τ_{FPOC} mostly depend on biologically mediated reactions, which rapidly respond to changes in hydroclimatic conditions and C inputs (Pearson's correlation coefficient of τ_{DOC} and τ_{FPOC} against aerobic and anaerobic respiration and, NPP, are either $R > 0.2$ or $R < -0.4$, Figure S4 in Supporting Information S1). In contrast, τ_{MAPOC} is mediated by abiotic processes and was not significantly correlated with precipitation, temperature, and NPP (Figure S4 in Supporting Information S1 and details in Section 2.3).

The greatest τ is located in the polar region (on average about 1,300 years) and continental region (on average about 500 years). These two regions have the greatest wetland SOC content with 80% of it consisting of MAPOC (Figure 1d). On average, the tropical region has the shortest τ of about 72 years despite having a large SOC content. In contrast, the arid region has the smallest SOC content (Figure 1b) but this region has an average τ of about 320 years (Figure 2b). Finally, MAPOC is remarkably stable across the five regions (Figure 2d). Panels b–e in Figure 2 show that different climatic regions and associated hydroclimatic conditions and land cover can determine variations in total SOC content and its allocations into FPOC and DOC, but not in MAPOC.

3.3. Long-Term Monthly Average τ of SOC, DOC, MAPOC, and FPOC

We next investigated the long-term monthly dynamics of τ of each SOC pool in the top one meter of soil. We found no substantial seasonal variation in τ of SOC in the tropical and arid regions (black lines in Figures 3a, 3b, 3f, and 3g). In contrast, we found monthly fluctuations up to one order of magnitude in the temperate, continental, and polar regions (Figures 3c, 3h, 3d, and 3e). The average monthly temperature varies substantially in those regions, and is significantly negatively correlated with τ ($R = -0.58$, $p < 0.01$, Figure S4 in Supporting Information S1). The large seasonal variability in τ in those regions is strongly supported by the model certainty analysis, where more than 70% of modeled grid cells having a certainty index $\Delta(m) \geq 0.75$ in month m signifies that the estimated τ is reliable (Figure S5 in Supporting Information S1). The monthly τ_{MAPOC} varies much less
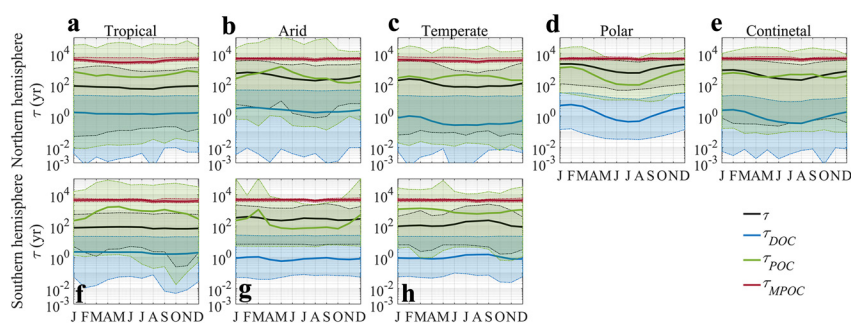
Figure 3. Long-term monthly average turnover time τ by climatic regions. Panels are organized by hemispheres (rows) and climatic regions (columns) for dissolved organic carbon τ_{DOC}, free particulate organic carbon τ_{FPOC}, and mineral-associated and protected organic carbon τ_{MAPOC}. Shaded areas represent the full range. The x-axis represents the months of the year, starting from January.

than τ and is not significantly correlated to temperature and precipitation (Figure 3, and correlation coefficient R in Figure S4 in Supporting Information S1). In contrast, τ_{DOC} is the shortest on average but with monthly variability of up to two orders of magnitude in the temperate, polar, and continental regions, and it is significantly negatively correlated to near-surface temperature ($R = -0.7$, $p < 0.01$, Figure S4 in Supporting Information S1). Overall, DOC content is between 0.5% and 6% of the total SOC, depending on the aboveground ecosystem (e.g., forest, grassland, and others) and the time of the year. In contrast, FPOC content is about 10%–25%. However, the turnover time of DOC is, on average, between two and three orders of magnitude faster than FPOC, hence the higher correlation in the overall turnover.

To uncover which C pool makes the largest contribution to the seasonality of SOC turnover, we examined the temporal variability of τ in each C pool. We found that on average $\tau_{MAPOC} > \tau_{FPOC}$ at all times and in all climatic regions, meaning that MAPOC and FPOC respond differently to environmental drivers. The reverse, $\tau_{MAPOC} < \tau_{FPOC}$, can occur locally as highlighted by the corresponding ranges (overlapped shaded areas in Figure 3), meaning that the MAPOC destabilization rate can become faster than losses of FPOC by biotic and abiotic processes. This condition occurred at least once per year in 12% of wetlands (by surface area) and can be explained by the large monthly variability in τ_{FPOC} being correlated to temperature ($R = -0.78$, $p < 0.01$) and NPP ($R = 0.37$, $p < 0.01$) as compared to no significant correlation of τ_{MAPOC} to the same environmental drivers. Hence, the overall τ of SOC is quantitatively dominated by τ_{MAPOC} but τ_{FPOC} and τ_{DOC} provides seasonal variation, implying that FPOC and DOC are susceptible to local hydroclimatic conditions and can ultimately contribute to seasonal C loss or gain in wetlands.

3.4. Seasonality in Biotic and Abiotic Processes Controlling τ

To further analyze the variability in τ and determine which process prevails in controlling τ of SOC at seasonal scales (Section 2), we ranked the intensity of aerobic and anaerobic soil respiration (biotic processes), C mineral association and destabilization rates, and leaching in the top one meter of soil (abiotic processes, Table S1 in Supporting Information S1). We found that τ in about 78% of global wetlands (about 2.96 Mkm^2) is mainly controlled by anaerobic respiration (methanogenesis), in about 15% (about 0.57 Mkm^2) by aerobic respiration, and in about 5% (about 0.15 Mkm^2) by destabilization from mineral association (Figure 4). τ in the arid region such as wetlands in continental and western Australia, and wetlands at latitudes above 60°N are mainly controlled by aerobic respiration and destabilization from mineral association (Figure 4).

The monthly τ is negatively correlated with the intensity of biotic and abiotic fluxes, with a correlation coefficient R ranging between -0.9 and -0.3 ($p < 0.01$) depending on the climatic region (Figure 4 and Figure S4 in Supporting Information S1). On average, anaerobic respiration overcomes the other fluxes throughout the year in all regions (Figure 5). In contrast, aerobic respiration remains nearly constant across the year. The tropical region has some of the greatest and nearly constant monthly fluxes leading to low variability and magnitude in τ (<60 years) compared to other regions (more than 80% of modeled grid cells have $\Delta(m) \geq 0.75$, Figure S5 in Supporting Information S1). The rates of C losses via leaching, mineral-association, sulfur reduction, denitrification, anaerobic respiration, and aerobic respiration in the arid, polar, and continental regions are almost two
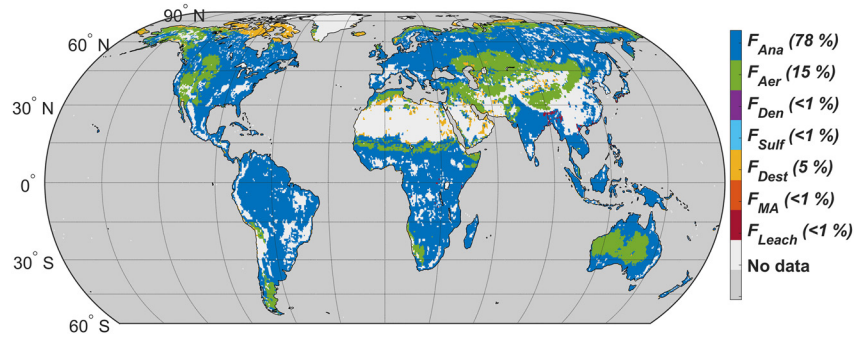
Figure 4. Geographic distribution of the dominant processes controlling τ of SOC. The dominant processes are defined as the main process affecting τ for more than 50% of the time for the period 2000–2017. F_{Leach}, F_{MA}, F_{Sulf}, F_{Den}, F_{Ana}, F_{Aer}, and F_{Dest} are the leaching, mineral-association, sulfur reduction, denitrification, anaerobic (methanogenic) respiration, aerobic respiration, and destabilization processes.

orders of magnitude smaller than in the tropical region, but these vary seasonally causing substantial variability in τ. Wetlands in arid and temperate regions show high monthly certainty ($\Delta(m) \geq 0.75$) in about 85% of wetlands (Figure S5 in Supporting Information S1), while continental and polar regions present variable certainty, with the least land area being certain during winters ($\Delta(m) < 0.75$, Figure S5 in Supporting Information S1).

Microbially mediated denitrification and sulfur reduction rates are nearly two to three orders of magnitude smaller than aerobic and anaerobic respiration. Among all abiotic processes, mineral association and leaching are the greatest and have nearly constant rates. However, the destabilization rates become larger during the summer months in the polar region (Figure 5), making substrate available to microbes to sustain either aerobic or anaerobic respiration. These results demonstrate the tight relationship between abiotic and biotic processes.

4. Discussion and Conclusion

Quantification of SOC stocks in wetlands at large spatial and temporal scales is a great challenge, and the quantification of their turnover time is especially challenging (Carvalhais et al., 2008, 2014; Y. Luo et al., 2016). The turnover time τ of a C pool can be associated with the level of activity of that pool, hence, conducting diagnostic analysis of how τ changes and the possible causes for those changes can shed light on the sensitivity of wetlands to climate change. However, a simplistic accounting of the C biogeochemistry can inflate uncertainty in C turnover, especially in the dimension of time if a steady-state is assumed and processes are not explicitly accounted for and tracked in time (He et al., 2016; Saunois et al., 2020; Todd-Brown et al., 2013; Wania et al., 2013). The approach we have developed within the hydrological and biogeochemical BRTSim-BAMS4 mechanistic model allowed us to track all C inputs and outputs for all the modeled SOC pools and determine their steady state (Section 2). Specifically, our modeling includes a detailed description of the coupled C, N, and S cycles,
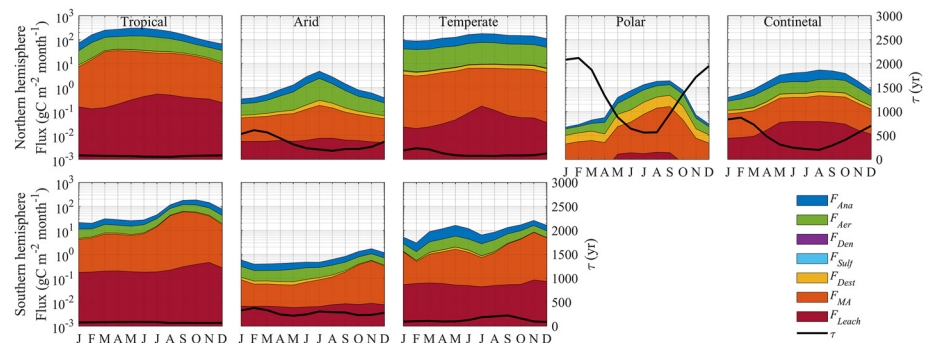
Figure 5. Long-term monthly average C fluxes and soil organic carbon turnover time τ. Panels are organized by hemispheres (rows) and climatic regions (columns). The fluxes are calculated as the wetland area weighted average. F_{Leach}, F_{MA}, F_{Sulf}, F_{Den}, F_{Ana}, F_{Aer}, and F_{Dest} are the leaching, mineral-association, sulfur reduction, denitrification, anaerobic (methanogenic) respiration, aerobic respiration, and destabilization cycles.

allowing us to estimate the size of each pool and track the C fluxes from one pool to another, as well as losses to the atmosphere and leaching below the first meter of soil explicitly in time and space. The pool sizes and fluxes were then used to calculate the turnover time with a new approach (Section 2) that extends the framework in Six and Jastrow (2002). That is, while previous assessments based on modeling (e.g., Earth System Models—ESMs) or observational data calculate the turnover as the ratio between the total soil organic carbon stock and NPP (Carvalhais et al., 2014; Todd-Brown et al., 2013), we took into mechanistic account individual biotic and abiotic processes and their response to environmental drivers. Because this approach is temporally and spatially explicit, we were able to study the transient dynamics of τ and the corresponding level of certainty for several SOC pools to infer how different biotic or abiotic drivers influence C turnover in wetlands, which is pivotal information under changing climatic conditions.

We estimated an average global wetland SOC turnover time of 400 years, in the first meter of soil. Our estimates have a certainty index of $\Delta(m) > 0.75$ in 79% (3.0 Mkm^2) of the average global wetland area (here wetland area changes over time). Although there is a wide consensus that wetlands have one of the slowest C turnovers among ecosystems due to ponding (Trumbore, 2000), the existing literature lacks detailed information on the SOC turnover of wetlands. Hence, our estimates have to be contextualized against ESMs modeling or observations of the turnover time not addressing wetlands explicitly, or including wetlands only implicitly within lumped ecosystems (He et al., 2016; Trumbore, 2000). For example, Todd-Brown et al. (2013) estimated a global average turnover time between 10.8 and 39.3 years within the first meter of soil (excluding wetlands descriptions) using 11 ESMs, while Z. Luo et al. (2019) estimated an average of 1,015 years in the subsoil by coupling multiple observation data sets with specific NPP allocations for above- and below-ground C inputs to soil (again not exclusively in wetlands). Note that these differences do not mean that our estimates have lower reliability, but rather that estimates refer to different ecosystems within the same unit area and come from two different approaches. Additionally, the methods deployed here have a substantially higher degree of process accounting and feedback.

Clearly, an explicit accounting of wetlands can lead to differences in τ as compared to other estimates not explicitly addressing wetlands. However, in general, there is a substantial inconsistency between $\Delta^{14}C$ observations in upland soil, which suggests turnover times in excess of thousand years (3,100 ± 1,800 years, He et al., 2016) as compared to modeling, which generally does not exceed 1,000 years (e.g., 10.8 and 39.3 years from ESMs and about 1,000 from Z. Luo et al. (2019)). These figures raise the question, how accurate is the representation of biogeochemical processes in models? Our work does not provide a perfect answer to this question but is the first attempt to increase the level of process accounting while testing modeling capabilities against independent observations that include biogeochemical reactions, GHG emissions, nutrient stocks, and sequestrations (Section 2). Specifically, biotic processes govern the C cycle in soil, causing substantial monthly variability in τ_{DOC} and τ_{FPOC}, particularly in temperate, continental, and polar regions, where temperature significantly changes seasonally.

The priming effect, which occurs when the addition of new labile C promotes microbial growth and increases the loss of carbon, is paramount to predicting C stocks and emissions due to land cover and climate changes, particularly under CO_2 fertilization, where aboveground biomass and mean soil inputs are enhanced (Guenet et al., 2018). While BAMS4 explicitly considers microbial dynamics, it does not include the priming effect as a separate process. Instead, the model output can reflect the priming effect as an outcome due to the inclusion of the complex feedback between different C pools and microbial functional groups in BAMS4. For example, our model outputs may indicate priming effects in conditions optimal for microbial growth (e.g., no water stress and warm climate), where the addition of labile C from root exudation increases microbial growth and biomass that subsequently speed up the aerobic respiration of DOC following the Michaelis-Menten-Monod kinetics. When the concentration of DOC decreases, MAPOC tends to be destabilized and transformed to the soluble form to re-balance the equilibrium reaction, causing a decrease of MAPOC. In the way our model is structured, this phenomenon may not happen in conditions not favorable for microbial growth. However, future model development should include the priming effect on MAOC turnover as a function of the ratio of labile (DOC) and recalcitrant (MAPOC) carbon input in soil for better accounting.

The leaching of carbon is an important environmental control, sometimes underestimated in C modeling that neglect advection-diffusion transport (He et al., 2016; Houlton et al., 2015; Zhu & Riley, 2015). The top one meter of wetlands is rich in C but is also highly susceptible to changes in C input and hydroclimatic variables because of the high C availability to microbes in the form of DOC and FPOC. Percolation below the root zone makes DOC inaccessible to microbes and prone to stabilization into mineral soil particles (Sanderman &

Amundson, 2008), recharging deep C stocks. The subsoil stores a high organic C stock in the form of MAPOC (about 96%), which we found less susceptible to environmental changes, consistent with Witzgall et al. (2021) and Dungait et al. (2012). The lack of direct input of fresh organic C, which generally provides substrate to microbes, seems to enhance stability, however, changes in land management and soil use (e.g., wetlands draining and conversion to agriculture) may affect the C distribution in soil, resulting in destabilization and C losses. Hence, DOC leaching requires further investigation and quantification of its role in the global C cycle. Accounting for deep C leaching will allow for an assessment of the role of topsoil C losses that could be sequestered in deeper soil. Ultimately, the polar region shows a prevalent control on τ by destabilization (i.e., the release of mineral-associated C to aqueous C), particularly during summer, the period that coincides with the highest biotic activity and therefore highest C emissions (losses).

Global climate has experienced unprecedent warming and changes in precipitation patterns and depth (Salimi et al., 2021). These hydroclimatic changes may rise concern on the SOC cycle in polar, temperate, and continental regions, where τ changes between one or two order of magnitudes over the year due to seasonality. Warming climates result in longer periods of temperature in the microbes' optimum growth range, hence reducing τ (faster turnover). The greatest area of concern is the polar region, which has been a pristine sink of the largest amount of SOC (Lal, 2004), helping to buffer climate change. For example, Canada recorded an increase in annual average temperature of 1.7°C for the period 1948–2018, and model predictions draw an increase in the frequency of extreme events, particularly in the northern latitudes, with significantly more warming during the winter season than the summer (Berardi & Jones, 2022). Despite the current effort of the scientific community in understanding C-climate feedback, the fate of C under variable climatic stressors remains relatively uncertain in this region, though a greater likelihood for microbial decomposition rate to exceed above ground biomass production is expected. This possibly shifts the system from C sink to GHG source.

5. Limitation of This Work

We acknowledge limitations of our framework regarding the turnover time estimates. The chosen resolution is a key factor; at the current resolution, an area of 50 × 50 km is modeled under the same hydroclimatic and soil biogeochemical conditions. However, only a fraction of that area is flooded. The fluxes presented in this work are calculated based on the actual wetland extension each month, however, the water table is homogenously solved in each grid cell. This can lead to a poor description of the actual redox conditions of the soil, which may introduce errors in estimated aerobic and anaerobic respiration. The modeling framework does not include soil erosion and fires that enhance C loss, and the ice thaw-freeze cycle that can change the microbial response and community composition (Ji et al., 2022).

Additionally, this study does not include local landscape heterogeneity and microtopography because of the coarse resolution (~2,500 km^2 area each grid cell), which may give rise to errors and underestimate the leaching of C from/into wetlands. Although soil moisture and water table dynamics modeling at high-resolution has been recently tested (~1 km, e.g., Miguez-Macho et al., 2008), most of the current regional and global scale modeling frameworks do not account for microtopography, connectivity, and lateral fluxes and their effects on the nutrient cycles because the inclusion of these factors requires the model to be run on a much finer spatial resolution that leads to a high computational demand. An optimized framework that merges surface hydrology and biogeochemical models without requiring a high computational cost should be prioritized.

Data Availability Statement

The georeferenced data on SOC pool size and turnover time are distributed via *figshare* at https://doi.org/10.6084/m9.figshare.20099462 (Pasut, 2023).

Code Availability: The BRTSim software used in this work is available under CC BY 4.0 International Licence at https://sites.google.com/site/thebrtsimproject. An example of input files required to run the model can be downloaded via *figshare* at https://doi.org/10.6084/m9.figshare.20099462 (Pasut, 2023).

References

Berardi, U., & Jones, S. (2022). The efficiency and GHG emissions of air source heat pumps under future climate scenarios across Canada. *Energy and Buildings*, *262*, 112000. https://doi.org/10.1016/j.enbuild.2022.112000

Boon, B., & Laudelout, H. (1962). Kinetics of nitrite oxidation by *Nitrobacter winogradskyi*. *Biochemical Journal*, *85*(3), 440–447. https://doi.org/10.1042/bj0850440

Bréchet, L., Le Dantec, V., Ponton, S., Goret, J.-Y., Sayer, E., Bonal, D., et al. (2017). Short- and long-term influence of litter quality and quantity on simulated heterotrophic soil respiration in a lowland tropical forest. *Ecosystems*, *20*(6), 1190–1204. https://doi.org/10.1007/s10021-016-0104-x

Brooks, R., & Corey, A. (1964). *Hydraulic properties of porous media. Hydrology Paper No. 3*. Civil Engineering Department, Colorado State University.

Calabrese, S., Garcia, A., Wilmoth, J. L., Zhang, X., & Porporato, A. (2021). Critical inundation level for methane emissions from wetlands. *Environmental Research Letters*, *16*(4), 044038. https://doi.org/10.1088/1748-9326/abedea

Canadell, J., Jackson, R. B., Ehleringer, J. B., Mooney, H. A., Sala, O. E., & Schulze, E.-D. (1996). Maximum rooting depth of vegetation types at the global scale. *Oecologia*, *108*(4), 583–595. https://doi.org/10.1007/BF00329030

Carvalhais, N., Forkel, M., Khomik, M., Bellarby, J., Jung, M., Migliavacca, M., et al. (2014). Global covariation of carbon turnover times with climate in terrestrial ecosystems. *Nature*, *514*(7521), 213–217. https://doi.org/10.1038/nature13731

Carvalhais, N., Reichstein, M., Seixas, J., Collatz, G. J., Pereira, J. S., Berbigier, P., et al. (2008). Implications of the carbon cycle steady state assumption for biogeochemical modeling performance and inverse parameter retrieval. *Global Biogeochemical Cycles*, *22*(2). https://doi.org/10.1029/2007GB003033

Chang, K.-Y., Riley, W., Collier, N., McNicol, G., Fluet-Chouinard, E., Knox, S., et al. (2021). Multi-model ensemble does not fill the gaps in sparse wetland methane observations, B35H–1513.

Cotrufo, M. F., Ranalli, M. G., Haddix, M. L., Six, J., & Lugato, E. (2019). Soil carbon storage informed by particulate and mineral-associated organic matter. *Nature Geoscience*, *12*(12), 989–994. https://doi.org/10.1038/s41561-019-0484-6

Dai, Y., Shangguan, W., Duan, Q., Liu, B., Fu, S., & Niu, G. (2013). Development of a China dataset of soil hydraulic parameters using pedotransfer functions for land surface modeling. *Journal of Hydrometeorology*, *14*(3), 869–887. https://doi.org/10.1175/JHM-D-12-0149.1

Dungait, J. A. J., Hopkins, D. W., Gregory, A. S., & Whitmore, A. P. (2012). Soil organic matter turnover is governed by accessibility not recalcitrance. *Global Change Biology*, *18*(6), 1781–1796. https://doi.org/10.1111/j.1365-2486.2012.02665.x

Dutta, H., & Dutta, A. (2016). The microbial aspect of climate change. *Energy, Ecology and Environment*, *1*(4), 209–232. https://doi.org/10.1007/s40974-016-0034-7

Feir-Walsh, B. J., & Toothaker, L. E. (1974). An empirical comparison of the ANOVA F-test, normal scores test and Kruskal-Wallis test under violation of assumptions. *Educational and Psychological Measurement*, *34*(4), 789–799. https://doi.org/10.1177/001316447403400406

Golchin, A., Oades, J., Skjemstad, J., & Clarke, P. (1994). Soil structure and carbon cycling. *Soil Research*, *32*(5), 1043. https://doi.org/10.1071/SR9941043

Guenet, B., Camino-Serrano, M., Ciais, P., Tifafi, M., Maignan, F., Soong, J. L., & Janssens, I. A. (2018). Impact of priming on global soil carbon stocks. *Global Change Biology*, *24*(5), 1873–1883. https://doi.org/10.1111/gcb.14069

Guo, L. B., & Gifford, R. M. (2002). Soil carbon stocks and land use change: A meta analysis. *Global Change Biology*, *8*(4), 345–360. https://doi.org/10.1046/j.1354-1013.2002.00486.x

Harden, J. W., Trumbore, S. E., Stocks, B. J., Hirsch, A., Gower, S. T., O'neill, K. P., & Kasischke, E. S. (2000). The role of fire in the boreal carbon budget. *Global Change Biology*, *6*(S1), 174–184. https://doi.org/10.1046/j.1365-2486.2000.06019.x

Harris, I., Osborn, T. J., Jones, P., & Lister, D. (2020). Version 4 of the CRU TS monthly high-resolution gridded multivariate climate dataset. *Scientific Data*, *7*(1), 109. https://doi.org/10.1038/s41597-020-0453-3

Hättenschwiler, S., & Jørgensen, H. B. (2010). Carbon quality rather than stoichiometry controls litter decomposition in a tropical rain forest. *Journal of Ecology*, *98*(4), 754–763. https://doi.org/10.1111/j.1365-2745.2010.01671.x

He, Y., Trumbore, S. E., Torn, M. S., Harden, J. W., Vaughn, L. J. S., Allison, S. D., & Randerson, J. T. (2016). Radiocarbon constraints implyreduced carbon uptake by soilsduring the 21st century. *American Association for the Advancement of Science*, *353*(6306), 1419–1424. https://doi.org/10.1126/science.aad4273

Hondula, K. L., Jones, C. N., & Palmer, M. A. (2021). Effects of seasonal inundation on methane fluxes from forested freshwater wetlands. *Environmental Research Letters*, *16*(8), 084016. https://doi.org/10.1088/1748-9326/ac1193

Houlton, B. Z., Marklein, A. R., & Bai, E. (2015). Representation of nitrogen in climate change forecasts. *Nature Climate Change*, *5*(5), 398–401. https://doi.org/10.1038/nclimate2538

Ji, X., Liu, M., Yang, J., & Feng, F. (2022). Meta-analysis of the impact of freeze–thaw cycles on soil microbial diversity and C and N dynamics. *Soil Biology and Biochemistry*, *168*, 108608. https://doi.org/10.1016/j.soilbio.2022.108608

Jobbágy, E. G., & Jackson, R. B. (2000). The vertical distribution of soil organic carbon and its relation to climate and vegetation. *Ecological Applications*, *10*(2), 423–436. https://doi.org/10.1890/1051-0761(2000)010[0423:TVDOSO]2.0.CO;2

Kirschbaum, M. U. F. (2000). Will changes in soil organic carbon act as a positive or negative feedback on global warming (p. 32).

Kottek, M., Grieser, J., Beck, C., Rudolf, B., & Rubel, F. (2006). World map of the Köppen-Geiger climate classification updated. *Meteorologische Zeitschrift*, *15*(3), 259–263. https://doi.org/10.1127/0941-2948/2006/0130

Lal, R. (2004). Soil carbon sequestration to mitigate climate change. *Geoderma*, *123*(1), 1–22. https://doi.org/10.1016/j.geoderma.2004.01.032

Lavallee, J. M., Soong, J. L., & Cotrufo, M. F. (2020). Conceptualizing soil organic matter into particulate and mineral-associated forms to address global change in the 21st century. *Global Change Biology*, *26*(1), 261–273. https://doi.org/10.1111/gcb.14859

Luo, Y., Ahlström, A., Allison, S. D., Batjes, N. H., Brovkin, V., Carvalhais, N., et al. (2016). Toward more realistic projections of soil carbon dynamics by Earth system models. *Global Biogeochemical Cycles*, *30*(1), 40–56. https://doi.org/10.1002/2015GB005239

Luo, Z., Wang, G., & Wang, E. (2019). Global subsoil organic carbon turnover times dominantly controlled by soil properties rather than climate. *Nature Communications*, *10*(1), 3688. https://doi.org/10.1038/s41467-019-11597-9

Macdonald, J. A., Fowler, D., Hargreaves, K. J., Skiba, U., Leith, I. D., & Murray, M. B. (1998). Methane emission rates from a northern wetland; response to temperature, water table and transport. *Atmospheric Environment*, *32*(19), 3219–3227. https://doi.org/10.1016/S1352-2310(97)00464-0

Maggi, F. (2021). BRTSim. A general-purpose computational solver for hydrological, biogeochemical, and ecosystem dynamics. *25*.

Michealis, L., & Menten, M. (1913). Die kinetik der invertinwirkung. *Biochemische Zeitschrift*, *49*(333–369), 352.

Miguez-Macho, G., Li, H., & Fan, Y. (2008). Simulated water table and Soil moisture climatology over North America. *Bulletin of the American Meteorological Society*, *89*(5), 663–672. https://doi.org/10.1175/BAMS-89-5-663

Monod, J. (1966). From enzymatic adaptation to allosteric transitions. *American Association for the Advancement of Science*, *154*(3748), 475–483. https://doi.org/10.1126/science.154.3748.475

Pasut, C. (2023). The seasonality of biotic and abiotic processes controls the turnover of organic matter in wetlands [Dataset]. Figshare. https://doi.org/10.6084/m9.figshare.20099462

Pasut, C., Tang, F. H. M., Hamilton, D., Riley, W. J., & Maggi, F. (2021). Spatiotemporal assessment of GHG emissions and nutrient sequestration linked to agronutrient runoff in global wetlands. *Global Biogeochemical Cycles*, *35*(4), e2020GB006816. https://doi.org/10.1029/2020GB006816

Paul, E. A. (2014). *Soil microbiology, ecology and biochemistry*. Academic Press.

Pei, G., Liu, J., Peng, B., Gao, D., Wang, C., Dai, W., et al. (2019). Nitrogen, lignin, C/N as important regulators of gross nitrogen release and immobilization during litter decomposition in a temperate forest ecosystem. *Forest Ecology and Management*, *440*, 61–69. https://doi.org/10.1016/j.foreco.2019.03.001

Poggio, L., de Sousa, L. M., Batjes, N. H., Heuvelink, G. B. M., Kempen, B., Ribeiro, E., & Rossiter, D. (2021). SoilGrids 2.0: Producing soil information for the globe with quantified spatial uncertainty. *Soil*, *7*(1), 217–240. https://doi.org/10.5194/soil-7-217-2021

Poulter, B., Bousquet, P., Canadell, J. G., Ciais, P., Peregon, A., Saunois, M., et al. (2017). Global wetland contribution to 2000–2012 atmospheric methane growth rate dynamics. *Environmental Research Letters*, *12*(9), 094013. https://doi.org/10.1088/1748-9326/aa8391

Rallison, R. E. (1980). Origin and evolution of the SCS runoff equation.

Riley, W. J., Maggi, F., Kleber, M., Torn, M. S., Tang, J. Y., Dwivedi, D., & Guerry, N. (2014). Long residence times of rapidly decomposable soil organic matter: Application of a multi-phase, multi-component, and vertically resolved model (BAMS1) to soil carbon dynamics. *Geoscientific Model Development*, *7*(4), 1335–1355. https://doi.org/10.5194/gmd-7-1335-2014

Rittmann, B. E., & McCarty, P. L. (2001). Environmental biotechnology: Principles and applications.

Rodell, M., Houser, P. R., Jambor, U., Gottschalck, J., Mitchell, K., Meng, C.-J., et al. (2004). The global land data assimilation system. *Bulletin of the American Meteorological Society*, *85*(3), 381–394. https://doi.org/10.1175/BAMS-85-3-381

Rouifed, S., Handa, I. T., David, J.-F., & Hättenschwiler, S. (2010). The importance of biotic factors in predicting global change effects on decomposition of temperate forest leaf litter. *Oecologia*, *163*(1), 247–256. https://doi.org/10.1007/s00442-009-1528-1

Salimi, S., Almuktar, S. A. A. A. N., & Scholz, M. (2021). Impact of climate change on wetland ecosystems: A critical review of experimental wetlands. *Journal of Environmental Management*, *286*, 112160. https://doi.org/10.1016/j.jenvman.2021.112160

Sanderman, J., & Amundson, R. (2008). A comparative study of dissolved organic carbon transport and stabilization in California forest and grassland soils. *Biogeochemistry*, *89*(3), 309–327. https://doi.org/10.1007/s10533-008-9221-8

Saunois, M., Stavert, A. R., Poulter, B., Bousquet, P., Canadell, J. G., Jackson, R. B., et al. (2020). The global methane budget 2000–2017. *Earth System Science Data*, *12*(3), 1561–1623. https://doi.org/10.5194/essd-12-1561-2020

Scharlemann, J. P., Tanner, E. V., Hiederer, R., & Kapos, V. (2014). Global soil carbon: Understanding and managing the largest terrestrial carbon pool. *Carbon Management*, *5*(1), 81–91. https://doi.org/10.4155/cmt.13.77

Schroeder, R., McDonald, K. C., Chapman, B. D., Jensen, K., Podest, E., Tessler, Z. D., et al. (2015). Development and evaluation of a multi-year fractional surface water data set derived from active/passive microwave remote sensing data. *Remote Sensing*, *7*(12), 16688–16732. Article 12. https://doi.org/10.3390/rs71215843

Seiji, Y., Hideaki, K., Tsuyoshi, K., Naga, O., Kohei, Y., Shogo, U., et al. (2019). *The meteorological research institute Earth system model version 2.0, MRI-ESM2.0: Description and basic evaluation of the physical component* (pp. 2019–2051). 気象集誌. 第2輯, advpub. https://doi.org/10.2151/jmsj.2019-051

Six, J., & Jastrow, J. D. (2002). Organic matter turnover. *Encyclopedia of Soil Science*, *10*.

Snowdon, P., & Ryan, P. J. (2005). *Review of C: N ratios in vegetation, litter and soil under Australian native forests and plantations*. [Report -Australian Greenhouse Office] (p. 57). CSIRO.

Sulla-Menashe, D., Gray, J. M., Abercrombie, S. P., & Friedl, M. A. (2019). Hierarchical mapping of annual global land cover 2001 to present: The MODIS Collection 6 Land Cover product. *Remote Sensing of Environment*, *222*, 183–194. https://doi.org/10.1016/j.rse.2018.12.013

Temmink, R. J. M., Lamers, L. P. M., Angelini, C., Bouma, T. J., Fritz, C., van de Koppel, J., et al. (2022). Recovering wetland biogeomorphic feedbacks to restore the world's biotic carbon hotspots. *Science*, *376*(6593), eabn1479. https://doi.org/10.1126/science.abn1479

Todd-Brown, K. E. O., Randerson, J. T., Post, W. M., Hoffman, F. M., Tarnocai, C., Schuur, E. A. G., & Allison, S. D. (2013). Causes of variation in soil carbon simulations from CMIP5 Earth system models and comparison with observations. *Biogeosciences*, *10*(3), 1717–1736. https://doi.org/10.5194/bg-10-1717-2013

Trumbore, S. (2000). Age of soil organic matter and soil respiration: Radiocarbon constraints on belowground C dynamics. *Ecological Applications*, *10*(2), 399–411. https://doi.org/10.1890/1051-0761(2000)010[0399:AOSOMA]2.0.CO;2

Walter, B. P., Heimann, M., & Matthews, E. (2001). Modeling modern methane emissions from natural wetlands: 1. Model description and results. *Journal of Geophysical Research*, *106*(D24), 34189–34206. https://doi.org/10.1029/2001JD900165

Wania, R., Melton, J. R., Hodson, E. L., Poulter, B., Ringeval, B., Spahni, R., et al. (2013). Present state of global wetland extent and wetland methane modelling: Methodology of a model inter-comparison project (WETCHIMP). *Geoscientific Model Development*, *6*(3), 617–641. https://doi.org/10.5194/gmd-6-617-2013

Wickland, K. P., & Neff, J. C. (2008). Decomposition of soil organic matter from boreal black spruce forest: Environmental and chemical controls. *Biogeochemistry*, *87*(1), 29–47. https://doi.org/10.1007/s10533-007-9166-3

Witzgall, K., Vidal, A., Schubert, D. I., Höschen, C., Schweizer, S. A., Buegger, F., et al. (2021). Particulate organic matter as a functional soil component for persistent soil organic carbon. *Nature Communications*, *12*(1), 4115. https://doi.org/10.1038/s41467-021-24192-8

Zhang, Y., Pena Arancibia, J., McVicar, T., Chiew, F., Vaze, J., Zheng, H., & Wang, Y. (2016). *Monthly global observation-driven Penman-Monteith-Leuning (PML) evapotranspiration and components. V2*. CSIRO.

Zhang, Z., Fluet-Chouinard, E., Jensen, K., McDonald, K., Hugelius, G., Gumbricht, T., et al. (2021). Development of the global dataset of Wetland Area and Dynamics for Methane Modeling (WAD2M). *Earth System Science Data*, *13*(5), 2001–2023. https://doi.org/10.5194/essd-13-2001-2021

Zhu, Q., & Riley, W. J. (2015). Improved modelling of soil nitrogen losses. *Nature Climate Change*, *5*(8), 705–706. https://doi.org/10.1038/nclimate2696